Research Article | Vol. 29, No. 4 / 15 February 2021 / Optics Express 5982
Optics EXPRESS

High-order parametric generation of coherent XUV radiation

O. Hort,[1,2,3,*] A. Dubrouil,[1,4] M. A. Khokhlova,[5,6] D. Descamps,[1] S. Petit,[1] F. Burgy,[1] E. Mével,[1] E. Constant,[1,7] and V. V. Strelkov[8,9]

[1]Université de Bordeaux, CNRS, CEA, Centre Laser Intenses et Applications (CELIA), 43 rue P. Noailles, 33400 Talence, France
[2]Photonics Institute, Vienna University of Technology, Gusshausstraße 27, A- 1040 Vienna, Austria
[3]ELI Beamlines, FZU – Institute of Physics of the Czech Academy of Sciences, Na Slovance 1999/2, 182 21 Praha 8, Czech Republic
[4]Currently with Femtoeasy, Femto Easy SAS, Bât. Gienah, Cité de la Photonique, 11 avenue de Canteranne, 33600 Pessac, France
[5]Max Born Institute for Nonlinear Optics and Short Pulse Spectroscopy, Max-Born-Straße 2A, Berlin 12489, Germany
[6]Blackett Laboratory, Imperial College London, South Kensington Campus, London SW7 2AZ, United Kingdom
[7]Université de Lyon, Université Claude Bernard Lyon 1, CNRS, Institut Lumière Matière (ILM), 69622 Villeurbanne, France
[8]Prokhorov General Physics Institute of the Russian Academy of Sciences, 38 Vavilova Street, Moscow 119991, Russia
[9]Moscow Institute of Physics and Technology (State University), Dolgoprudny, Moscow Region 141700, Russia
*ondrej.hort@eli-beams.eu

Abstract: Extreme ultraviolet (XUV) radiation finds numerous applications in spectroscopy. When the XUV light is generated via high-order harmonic generation (HHG), it may be produced in the form of attosecond pulses, allowing access to unprecedented ultrafast phenomena. However, the HHG efficiency remains limited. Here we present an observation of a new regime of coherent XUV emission which has a potential to provide higher XUV intensity, vital for applications. We explain the process by high-order parametric generation, involving the combined emission of THz and XUV photons, where the phase matching is very robust against ionization. This introduces a way to use higher-energy driving pulses, thus generating more XUV photons.

© 2021 Optical Society of America under the terms of the OSA Open Access Publishing Agreement

1. Introduction

In recent decades, X-ray free-electron lasers (FEL), synchrotrons, and laser-driven XUV and X-ray sources, have become the most widespread generators of coherent and ultrashort pulse radiation in this spectral range [1–4], and are used for various applications in physical chemistry, atomic physics and coherent imaging [5–7]. Among the laser-driven sources, high-order harmonic generation (HHG) in gases achieves very good spatial and temporal coherence, stability and setup compactness when compared to X-ray FEL and synchrotrons [8–12]. However, HHG suffers from poor conversion efficiency resulting in low XUV photons number. This limits the interdisciplinary spread of XUV applications.

The effort to increase the generated XUV signal has resulted in number of methods addressing amelioration of the phase matching, exploiting quasi-phase-matching, low-order wave mixing or even XUV amplification [13–16]. A different way was opened by defining the scaling laws [17] in combination with recent technological advances in Ti:Sapphire and OPCPA-based laser chains [18,19]. Such systems reach high pulse energy at higher repetition rates than before allowing

#418449 https://doi.org/10.1364/OE.418449
Journal © 2021 Received 8 Jan 2021; accepted 1 Feb 2021; published 9 Feb 2021

Optics EXPRESS

generation of high XUV photon numbers suitable for applications even with state-of-the-art HHG conversion efficiency.

Here we present the experimental and theoretical study of the high driving intensity regime of HHG and observed parametric generation of XUV radiation. We found that this new XUV source signal keeps rising at driving intensities where standard HHG saturates. Therefore, it introduces a way to significantly increase XUV signal for photon-hungry applications across various science fields.

2. Experimental observation

We generate XUV radiation in gases with a Ti:Sapphire laser in a loose focusing geometry at high intensity and characterize, spatially and spectrally, the emitted XUV light. We use multi-mJ TW pulses of 45 fs duration centered at 810 nm with a spatially-filtered beam and we detect the short quantum trajectory only (for details, see Supplement 1).

Figure 1 shows the XUV spectra obtained in krypton gas jet at different driving laser intensities. Conventional high-order harmonics (HH) appear at low intensity and red-side satellites (RSS) appear on the low-frequency side of the harmonic peaks when high driving intensities are used (see Supplement 1 for the full dataset).

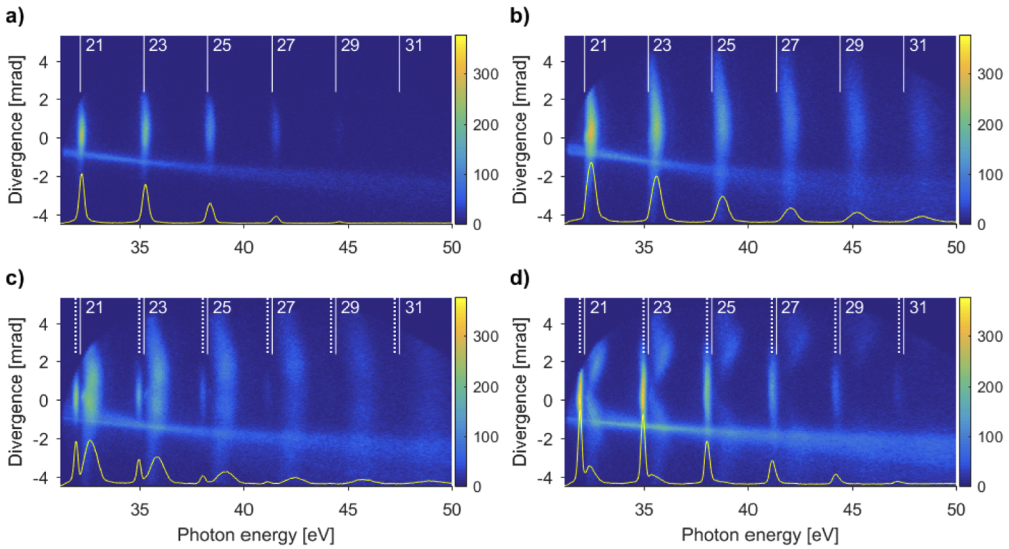


Fig. 1. Experimental spatially-resolved XUV spectra generated in a krypton jet. The colorbar shows spatio-spectral intensity (in arbitrary units). The reference photon energy $q\omega_0$ of the HH (generated at low intensity) is presented by the solid white lines, while the photon energy of the RSS given by Eq. (1) with the parameters $Q = 27$ and $m = 2$ (see below) are shown by dashed lines. Solid yellow lines present integrated on-axis XUV signal in the full angle of 1.5 mrad (plotted in arbitrary units and arbitrary offset). The driving laser intensities (estimated for propagation under vacuum) are 0.15, 0.71, 2.9, and 3.5×10^{15}W/cm^2 from (a) to (d) correspondingly.

At a low driving intensity of 0.15×10^{15} W/cm^2 (Fig. 1(a)), the harmonics are spectrally symmetric with a low spatial divergence and the peaks are located at photon energy $q\omega_0$ with only a small blue shift. The highest generated harmonic is HH29. With a higher driving intensity (Fig. 1(b)) the cutoff rises and there is a pronounced blue shift and spectral asymmetry of the harmonics. The asymmetry is due to the ionization of the generating medium that confines HHG in the pulse rising front and the blue shift is due to IR pulse propagation in the ionized medium

Optics EXPRESS

that shifts the laser central frequency. Simultaneously the XUV beam divergence increases with driving intensity.

At a high driving intensity of 2.9×10^{15} W/cm^2 (Fig. 1(c)), additional peaks, here referred to as RSS, appear on the red side of harmonics. At a very high driving intensity (Fig. 1(d)), the RSS signal further increases. All RSS peaks are red-shifted as compared to the spectral position of the harmonics generated at very low laser intensities and exhibit a lower spatial divergence. In general, with increasing driving intensity, additional RSS appear near harmonics of higher order. This behavior presents itself as a cutoff that rises with the driving laser intensity.

The HH and RSS signals evolve in different ways. To illustrate this we show in Fig. 2 the measured XUV signal on axis as a function of driving intensity corresponding to Fig. 1.

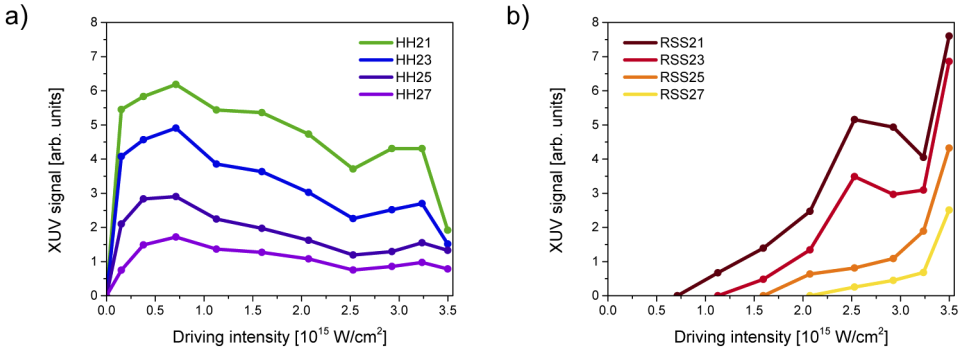


Fig. 2. Experimental comparison of the on-axis XUV signal (spatially integrated in the full angle of 0.5 mrad around optical axis) of the (a) HH and (b) RSS peaks as a function of the driving laser intensity.

With increasing driving intensity the HH signal rises up to saturation at 0.7×10^{15} W/cm^2 and then starts to decrease slowly. This is attributed to a degradation of the phase-matching conditions for HHG and high ionization of the medium modulating the spatio-temporal profile of the IR pulse [20,21]. In contrast, the RSS signal first appears only around 1.2×10^{15} W/cm^2 and *continues to grow* with an increase in driving intensity. It does not reach saturation and its evolution is qualitatively very different to HH signal. At intensities above 3.25×10^{15} W/cm^2 the RSS peaks are of similar or higher on-axis brightness than those of the HH. As mentioned above, there is a threshold driving intensity for every RSS order that increases with the order (RSS cutoff).

The spatial profile and spectral width of the RSS differ significantly from the ones of the HH beam. Figure 3(a) presents the spatial divergence of the HH and RSS beams as a function of the driving laser intensity. The HH divergence increases quickly with intensity up to 0.7×10^{15} W/cm^2. Then its spatial profile keeps widening up to the high intensity of 3.5×10^{15} W/cm^2 where it becomes very irregular, with its size comparable to that of the 40 mm MCP detector diameter. On the contrary, the divergence of the RSS beam is lower than the HH beam and does not change much with the driving laser intensity over a large range of intensities up to 2.9×10^{15} W/cm^2. Above this, the RSS beam expands while keeping a regular spatial profile.

Figure 3(b) shows the spectral width corresponding to Fig. 1. The spectral width of the RSS is close to that of the HH for the lowest driving intensity, and significantly lower for the higher ones. Moreover, the RSS frequency does not shift or broaden substantially with the increase of the driving intensity, even when the gas medium becomes strongly ionized.

From Figs. 1, 2 and 3 it is clear that the HH and RSS peaks behave differently. Moreover, the spectrum and the beam shape of the RSS radiation do not depend on the gas pressure in the

Optics EXPRESS

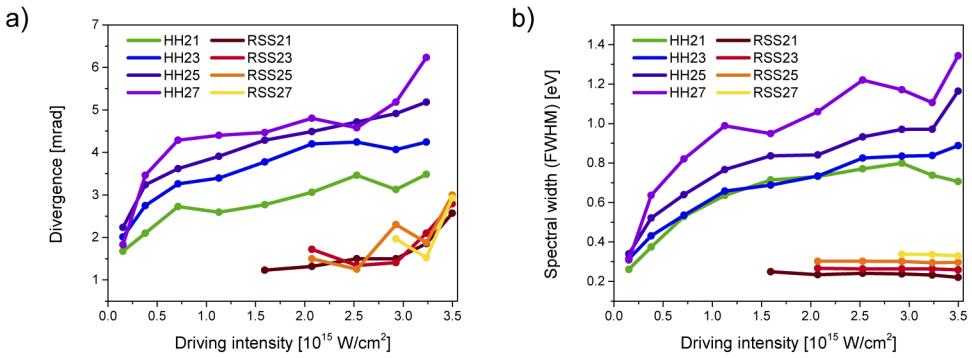


Fig. 3. XUV beam (a) divergence and (b) spectral width measured at FWHM of the HH and RSS as functions of the driving laser intensity.

generating medium while those of HH do (Figure S1 in Supplement 1). This implies that HH and RSS originate from different processes.

3. General properties

The features observed in our experiments are consistent with the HPG process that was recently predicted by V. Strelkov [22]. This process is analogous to well-known (low-order) parametric generation but it involves many laser photons corresponding to the intense-field domain. While in HHG several laser photons turn into a single XUV photon, in the high-order parametric process they transform into few photons generated in a different spectral range (XUV to THz), see Fig. 4.

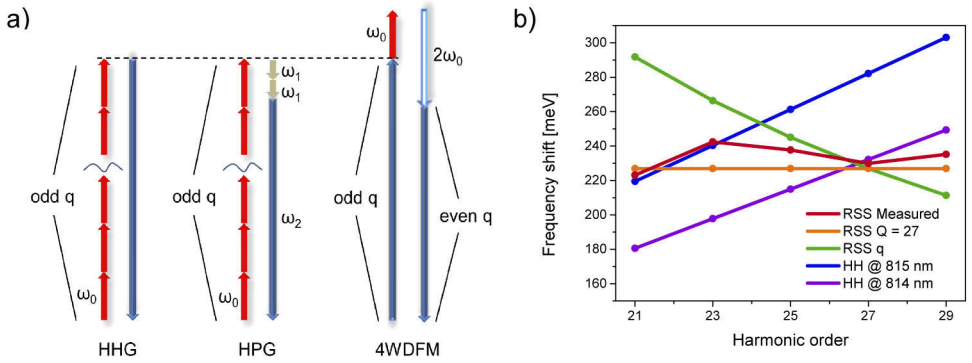


Fig. 4. (a) Schematic comparison of nonlinear processes which lead to coherent XUV emission: HHG, HPG (with $m = -2$) and four-wave difference-frequency mixing (4WDFM) [15]. (b) Measured RSS photon energy shifts from the exact energies of HH of the 810 nm laser wavelength (red), compared to values calculated (1) using the mean-plateau harmonic order $Q = 27$ (orange) and using harmonic orders q (green). The photon energy shifts of HH for the hypothetical driving central frequencies of 815 nm (blue) and 814 nm (purple) are included to prove that RSS energy shifts are incompatible with those of HH of a red-shifted driver. (The 814 and 815 nm are arbitrarily chosen to allow simple comparison of the RSS with HH generated by longer fundamental wavelength.)

The nature of the nonlinearity leading to HHG and HPG is the same, just as low-order nonlinearity of a crystal can lead to low-order harmonic generation or parametric generation, depending on the experimental conditions. In our case the origin of the high-order nonlinearity

Optics EXPRESS

is a rescattering process [10] so both HHG and HPG take place at similar laser intensities above a threshold driving intensity. This threshold is a consequence of minimal number of IR photons needed for the process.

Similar to low-order parametric generation, the value of the generated frequencies of idler and signal is defined by phase-matching conditions. In our case the parametric process leads to generation of the XUV photons with lower photon energy than the HH photons have and therefore these appear at the red side of the harmonics in the spectrum. The frequency ω_2 of this parametric signal is:

$$\omega_2 = q\omega_0 + m\omega_1, \tag{1}$$

where ω_0 is the driving laser frequency, q is the harmonic order, m is a negative low even number and ω_1 denotes the idler frequency. Although many frequencies ω_1 and ω_2 can fulfill this relation, only specific ones can be generated and enhanced because of phase matching conditions as stated below.

It is shown in [22] that the HPG process can be more efficient than HHG, assuming that at high driving intensity the plasma dispersion provides the dominant contribution to the phase mismatch. In that case, the detuning from the phase-matching condition is $\Delta k = -\frac{\omega_{pl}^2}{2c}(\frac{q}{\omega_0} + \frac{m}{\omega_1} - \frac{1}{q\omega_0 + m\omega_1})$, where ω_{pl} is the plasma frequency, defined by the density of the free electrons in the generating gas. Thus for the idler frequency $\omega_1 = -\frac{\omega_0 m}{q}$ the HPG process is almost phase-matched *regardless of the electronic density* (see Fig. 5). This is very important because the latter naturally varies in space and time during the generation, and any phase mismatch significantly limits coherent XUV emission via HHG. We show this in Fig. 2, where the HH signal decreases with increasing IR intensity, and the RSS signal increases as a consequence of the phase-matched parametric process.

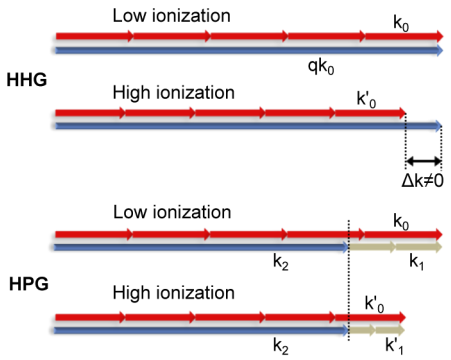


Fig. 5. Schematic comparison of the HHG and HPG phase matching and blue shift with the presence of low and high ionization. The high electronic density creates a phase mismatch $\Delta k \neq 0$ in case of HHG. In the case of HPG, the change of the fundamental k_0 is compensated by the change of k_1 so $\Delta k = 0$ is valid even under high ionization and the RSS (wave number k_2) are phase-matched and keep their spectral frequency.

For the lowest order ($m = -2$) of the idler emission, $\omega_1 = \frac{2\omega_0}{Q}$ (with $Q \approx q$) and it can contribute to the phase-matched emission of RSS frequency ω_2 given by Eq. (1). Figure 1 shows that this equation describes the HPG spectral frequency very well, assuming the lowest possible order $m = -2$ and choosing the order Q close to the mean value of the harmonic order in the plateau region. We stress here that the parameters m and Q cannot be chosen arbitrarily. Indeed, $m = -2$ is the most favorable for krypton and argon gas medium, as a parametric process in general is less efficient for higher parametric orders (i.e. higher absolute values of m). Our approach is similar towards the parameter Q. In [22] it is considered that every single

Optics EXPRESS

harmonic has its own RSS satellite, generated via specific ω_1. However, frequencies $\omega_1 = \frac{2\omega_0}{q}$ are very close to each other for neighbor harmonics. We assume that the identical idler frequency $\omega_1 = \frac{2\omega_0}{Q}$ is generated for all plateau orders. In this case all the harmonic orders would contribute to the generation of this frequency ω_1, so the parametric process becomes more efficient.

In our conditions the idler frequency ω_1 is in the spectral range of few tens of THz (27 THz corresponding for Fig. 1). Such kind of radiation can be created directly in the gas jet during the gas ionization. THz radiation was successfully generated in plasma produced by focusing high intensity femtosecond pulses into a gas target [23–30]. In these, it was shown (for a review see [26]) that an intense few-cycle laser pulse can generate a THz field because the ionization takes place at few half-cycles and electronic motion after ionization is asymmetric. However, a similar mechanism can be valid for a multi-cycle pulse as well, if it is very intense (namely, its peak intensity is much higher than the photoionization threshold intensity): the ionization takes place rapidly yet at the front of the pulse, thus the high ionization degree can occur during few half-cycles.

4. Analysis

4.1. Frequencies of the RSS spectral peaks

The HPG theoretical predictions are highly consistent with the experimental results. Remarkably, in contrast to published works (mentioned below), it produces spectral peaks for all the harmonic orders. In Fig. 4(b) we compare our experimentally measured RSS spectral frequency to the calculated values using different methods and different fundamental wavelengths. As explained above, using one Q parameter for neighboring harmonics leads to excellent agreement between the calculated and measured data. In contrast to this, the possibility of RSS being generated by other processes such as HHG of longer fundamental wavelength is ruled out.

4.2. Widths of the RSS spectral peaks

HPG also explains why the RSS spectral width is much lower than that of the HH. As the enhancement of the parametric signal is proportional to its original intensity, the most intense frequency component is the most enhanced. As a result, the RSS are spectrally narrow. Moreover, the blue shift acquired by the fundamental wave ω_0 during ionization is compensated by the blue shift of ω_1 during ionization, so the RSS spectrum centered at ω_2 does not shift with increase of driving laser intensity. To explain this in more detail let us denote the ionization-induced blue shift of the fundamental as $\Delta\omega_0$; the blue shift of the low-frequency (idler) field ω_1 is inversely proportional to its frequency: $\Delta\omega_1 = \frac{\Delta\omega_0 Q}{|m|}$. So for the polarization response at the RSS frequency given by Eq. (1) the blue shifts of the two generating waves compensate each other: $\Delta\omega_2 = q\Delta\omega_0 + m\frac{\Delta\omega_0 Q}{|m|} \approx 0$ (this compensation is similar to the phase mismatch compensation illustrated in Fig. 5). Opposite to this, the ionization-induced blue shift of the fundamental leads to the pronounced blue shift of the polarization response for the qth HH, equal to $q\Delta\omega_0$. Thus, the spectral broadening due to the blue shift is much more pronounced for the HH than for the RSS [31].

There is another mechanism of the spectral shift of the XUV generated due to HHG and HPG, namely, the polarization response phase dependence on the generating field(s) intensity. For the HHG this leads to the blue shift at the rising front of the pulse and the red shift at the falling front; however, the ionization temporally confines HHG to the rising front, so this blue-shift adds to the ionization-induced one, leading to a strong broadening of the HH. The HPG process is phase-matched even for a high ionization degree of the gas, so it takes place mainly near the maximum of the fundamental pulse where the temporal variation of the intensity vanishes. Thus the polarization phase dependence at this intensity does not lead to a pronounced frequency shift or broadening of the RSS.

Optics EXPRESS

The spectral width of the RSS is thus close to the inverse of the pulse duration, which does not change much with the fundamental intensity. In contrast to this, the HH is broadened due to the two mechanisms described above, and this broadening increases in line with the fundamental intensity. This considerations explain the experimental results presented in Fig. 3(b). The observed RSS spectral width corresponds to a transform-limited XUV pulse duration of approximately 7.7, 6.9, 6 and 5.4 fs for RSS orders 21, 23, 25 and 27 respectively, which is shorter than 45 fs of the fundamental pulse, as expected for a high-order nonlinear process.

4.3. Angular divergence of the XUV

The parametric XUV generation process also explains the narrow angular divergence of the XUV emission observed experimentally as shown in Fig. 3.

As discussed above, the generation of RSS is phase-matched regardless of the electronic density (in contrast to HHG, see Fig. 5). The RSS are therefore efficiently generated both on the optical axis and periphery of the fundamental beam resulting in large XUV beam size and low beam divergence in the far field, irrespective of the IR intensity. Note that, at low IR intensity when HHG also takes place on axis, the HH divergence is similar to that of RSS (see Fig. 3).

5. Numerical study

To verify our analysis of this process we solve numerically the 3D time-dependent Schrödinger equation (TDSE) for an atom in an external laser fundamental field and calculate the spectrum of the microscopic response (see Supplement 1 for more details).

When the fundamental intensity is so high that the ionization occurs during several half-cycles, a continuum spectrum in the multi-THz domain appears. While the microscopic response increases with decreasing frequency in the range of few tens of THz, frequencies below the plasma frequency (15 THz for plasma density 3×10^{18} cm^{-3}) cannot propagate in the plasma. Our calculations for argon show that the THz spectrum has a maximum between 20-30 THz and the intensity of this THz field grows very rapidly with the laser intensity when the latter is about 0.4×10^{15} W/cm^2 and then saturates.

Solving the propagation equation we find the macroscopic response of the medium. In our conditions the THz field of 27 THz spectral frequency (for $Q = 27$ and $m = -2$) reaches intensity of 10^{11} W/cm^2 after propagation of the half target length. Such THz intensity is significantly higher than the one originally assumed in [22]. So the HPG can take place for much shorter propagation distances and lower pressures, as confirmed by our results.

In our further calculations we study the XUV generation by the laser field and the THz field. Figure 6(a) shows the intensity of the harmonic and RSS as a function of the propagation distance. We see that the harmonic intensity behaves in agreement with numerous HHG studies [11,12,20,31]: first it grows quadratically and then saturates (note the log-log scale). However, the intensity of the RSS keeps almost quadratic growth through the full length of the simulation because of much better phase matching for the generation of the RSS. So after the propagation the RSS becomes significantly more intense than the harmonic. That corresponds to our experimental data on Fig. 2. Figure 6(b) presents the generated spectrum near the 17^{th} harmonic. One can see that the RSS line is narrower than the the harmonic line in agreement with Fig. 3(b). The origin of this narrowing for the process of HPG was discussed above.

Optics EXPRESS

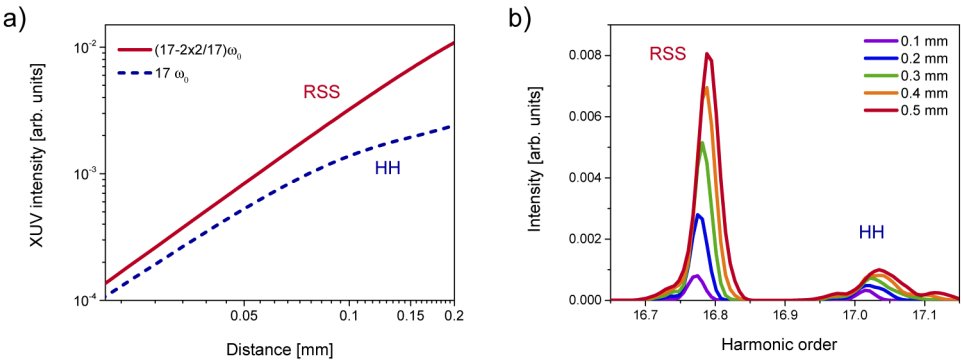


Fig. 6. (a) Calculated intensities of the 17^{th} HH and the same order RSS (corresponding to HPG on the frequency $17\omega_0$ - $2\omega_1$) as functions of the propagation distance in the generating gas medium in log-log scale. (b) Spectrum of the 17^{th} order of RSS and HH for several propagation distances in the generating medium. Calculation is done for argon, the gas density is 3×10^{18} cm^{-3}, laser intensity is 0.2×10^{15} W/cm^2.

6. Discussion

Many nonlinear processes occurring in a gas jet irradiated by a strong laser field leading to XUV light emission have already been reported. They all exhibit specific features that are not observed here and they cannot explain our observations. In the following paragraphs, we compare our experimental results with published findings.

The XUV spatio-spectral shape has been studied already in several papers [32–39] showing complex broadening and splitting of a harmonic line with an increase of the driving laser intensity. These studies demonstrated (i) *continuously* evolving XUV spectrum with increasing laser intensity and (ii) more pronounced spectral features for the lower harmonics and *progressive* disappearance of features for the higher ones. This behavior is very different from our observations, demonstrating the sudden appearance of the red-side peaks for high laser intensity, no pronounced evolution of their spectral frequency under further intensity increase and similar spectral frequency in the plateau and cut-off regions. Therefore, the explanation offered in [32–39] does not fit our case. Moreover, the intensities that we use here with Kr are higher than those used in the former studies and allow accessing new phenomena.

Another group of experiments reported the modification of the XUV spectrum due to resonances of the generating particles [40–46]. However, the resonance-induced modification of the spectrum is specific for each type of generating particles. In contrast to this, in our experiments spectral frequency of the RSS is robust and similar for different gases (Figs. S2-S6 in Supplement 1). So the observed spectral features cannot be attributed to resonances.

The publications reporting the amplification of XUV were focused on stimulated emission via population inversion [16,47] or other approaches using two-color [48,49] or single-color [50] driving field. In these papers the emission on HHG frequencies (or at corresponding combination of frequencies for the two-color case) have been studied, however the emission of *new* spectral components have not been reported, in contrast to this paper.

We also exclude various types of low-order wave mixing such as sum- or difference-frequency generation [15] because, in our case, there is no signal at even harmonic orders. Figure 4 also illustrates that the spectral frequency of the RSS does not correspond to an odd multiple of any infrared frequency. Therefore it cannot be due to HHG with a spectrally shifted pre- or post-pulse or a chirped pulse.

Optics EXPRESS

To the best of our knowledge, the HPG-like XUV spectra have not been reported, although our experimental conditions are within the reach of current technology. We believe that it is caused by the unique combination of our experimental parameters together with the fact, that we extensively study the experimental conditions that are believed to be inefficient for HHG. Our generating conditions are very specific in a way that the short medium in the high ionization regime is far above phase-matched HHG. Note, that the RSS can easily be misinterpreted with alignment problems or IR spectral splitting. However, our results clearly show that driving of HHG with a chirped pulse or a prepulse cannot lead to the generation of RSS.

7. Conclusion

In conclusion, we have observed spectrally narrow, low divergence XUV emission at high intensity driving pulses. With support of numerical simulations, we show that all features of this emission are consistent with high-order parametric emission, where an intense laser pulse can generate XUV and THz photons in a phase-matched process irrespective of the electron density. The observed parametric signal can exceed the on-axis signal of regular HHG because it rises at driving intensities where the HHG signal saturates, giving the possibility of upscaling, as illustrated here by our simulations. In this sense, with high energy/high peak power laser system, HPG can produce XUV radiation with higher brightness and intensity than HHG. Moreover, as the XUV spectral bandwidth of the RSS is of similar order as the HH, we expect that one can generate attosecond pulse train via HPG.

Furthermore, this XUV parametric process may be improved. In analogy with the better understood parametric processes in the visible and mid-IR range, we anticipate that manipulating the idler will provide numerous ways to enhance and control temporally and spatially this bright coherent XUV beam. Further increases of the driving pulse energy/intensity can be used to prove the scalability, and complete temporal characterization could give more insight into the process of HPG. Finally, as the spectro-spatial profile of the RSS is very regular and does not depend on the driving pulse intensity and ionization degree, the HPG can be more attractive than HHG even for applications where focusability into very small spot is crucial.

Funding. Royal Society (NF161013); H2020 Marie Skłodowska-Curie Actions (657272, 797688); European Social Fund (CZ.1.07/2.3.00/20.0279); European Regional Development Fund (CZ.02.1.01/0.0/0.0/16_019/0000789); Ministerstvo Školství, Mládeže a Tělovýchovy (LM2015065, LM2015083, LQ1606); Conseil Régional Aquitaine (COLA2 2-1-3-09010502, NASA 20101304005); Agence Nationale de la Recherche (09-BLAN-0031-02 Attowave, 10-IDEX-03-02); Laserlab-Europe (Laserlab Europe II, Laserlab Europe III); Russian Foundation for Basic Research (19-02-00739).

Acknowledgments. O.H. acknowledges financial supports from European Union's Horizon 2020 research and innovation programme under grant agreements No 657272 and 797688. M.K. acknowledges funding from the Alexander von Humboldt Foundation. E.C. acknowledges stimulating discussions with Stefan Skupin. V.S. acknowledges stimulating discussions with Sergey Popruzhenko. We are grateful to Rachael Jack for manuscript language revision.

Disclosures. The authors declare no conflicts of interest.

Supplemental document. See Supplement 1 for supporting content.

References

1. J. J. Rocca, "Table-top soft x-ray lasers," Rev. Sci. Instrum. **70**(10), 3799–3827 (1999).
2. H. Daido, "Review of soft x-ray laser researches and developments," Rep. Prog. Phys. **65**(10), 1513–1576 (2002).
3. F. Krausz and M. Ivanov, "Attosecond physics," Rev. Mod. Phys. **81**(1), 163–234 (2009).
4. B. W. J. McNeil and N. R. Thompson, "X-ray free-electron lasers," Nat. Photonics **4**(12), 814–821 (2010).
5. S. R. Leone and D. M. Neumark, "Attosecond science in atomic, molecular, and condensed matter physics," Faraday Discuss. **194**, 15–39 (2016).
6. H. Yun, S. J. Yun, G. H. Lee, and C. H. Nam, "High-harmonic spectroscopy of aligned molecules," J. Phys. B: At., Mol. Opt. Phys. **50**(2), 022001 (2017).
7. H. N. Chapman and K. A. Nugent, "Coherent lensless x-ray imaging," Nat. Photonics **4**(12), 833–839 (2010).
8. A. McPherson, G. Gibson, H. Jara, U. Johann, T. S. Luk, I. McIntyre, K. Boyer, and C. Rhodes, "Studies of multiphoton production of vacuum-ultraviolet radiation in the rare gases," J. Opt. Soc. Am. B **4**(4), 595–601 (1987).

Optics EXPRESS

9. M. Ferray, A. L'Huillier, X. Li, L. Lompre, G. Mainfray, and C. Manus, "Multiple-harmonic conversion of 1064 nm radiation in rare gases," J. Phys. B: At., Mol. Opt. Phys. **21**(3), L31–L35 (1988).
10. P. B. Corkum, "Plasma perspective on strong field multiphoton ionization," Phys. Rev. Lett. **71**(13), 1994–1997 (1993).
11. P. Balcou, P. Salieres, A. L'Huillier, and M. Lewenstein, "Generalized phase-matching conditions for high harmonics: The role of field-gradient forces," Phys. Rev. A **55**(4), 3204–3210 (1997).
12. E. Constant, D. Garzella, P. Breger, E. Mével, C. Dorrer, C. Le Blanc, F. Salin, and P. Agostini, "Optimizing high harmonic generation in absorbing gases: Model and experiment," Phys. Rev. Lett. **82**(8), 1668–1671 (1999).
13. A. Rundquist, C. G. Durfee, Z. Chang, C. Herne, S. Backus, M. M. Murnane, and H. C. Kapteyn, "Phase-matched generation of coherent soft x-rays," Science **280**(5368), 1412–1415 (1998).
14. X. Zhang, A. L. Lytle, T. Popmintchev, X. Zhou, H. C. Kapteyn, M. M. Murnane, and O. Cohen, "Quasi-phase-matching and quantum-path control of high-harmonic generation using counterpropagating light," Nat. Phys. **3**(4), 270–275 (2007).
15. L. Misoguti, I. P. Christov, S. Backus, M. M. Murnane, and H. C. Kapteyn, "Nonlinear wave-mixing processes in the extreme ultraviolet," Phys. Rev. A **72**(6), 063803 (2005).
16. T. Bredtmann, S. Patchkovskii, and M. Ivanov, "Strong-field assisted extreme-ultraviolet lasing in atoms and molecules," New J. Phys. **19**(7), 073011 (2017).
17. C. M. Heyl, H. Coudert-Alteirac, M. Miranda, M. Louisy, K. Kovács, V. Tosa, E. Balogh, K. Varjú, A. L'Huillier, A. Couairon, and C. L. Arnold, "Scale-invariant nonlinear optics in gases," Optica **3**(1), 75–81 (2016).
18. A. Nayak, I. Orfanos, I. Makos, M. Dumergue, S. Kühn, E. Skantzakis, B. Bodi, K. Varju, C. Kalpouzos, H. Banks, A. Emmanouilidou, D. Charalambidis, and P. Tzallas, "Multiple ionization of argon via multi-XUV-photon absorption induced by 20-GW high-order harmonic laser pulses," Phys. Rev. A **98**(2), 023426 (2018).
19. O. Hort, M. Albrecht, V. Nefedova, O. Finke, D. Mai, S. Reyné, F. Giambruno, F. Frassetto, L. Poletto, J. Andreasson, J. Gautier, S. Sebban, and J. Nejdl, "High-flux source of coherent XUV pulses for user applications," Opt. Express **27**(6), 8871–8883 (2019).
20. M. B. Gaarde, J. L. Tate, and K. J. Schafer, "Macroscopic aspects of attosecond pulse generation," J. Phys. B: At., Mol. Opt. Phys. **41**(13), 132001 (2008).
21. A. Dubrouil, O. Hort, F. Catoire, D. Descamps, S. Petit, E. Mével, V. Strelkov, and E. Constant, "Spatio–spectral structures in high-order harmonic beams generated with terawatt 10-fs pulses," Nat. Commun. **5**(1), 4637 (2014).
22. V. V. Strelkov, "High-order optical processes in intense laser field: Towards nonperturbative nonlinear optics," Phys. Rev. A **93**(5), 053812 (2016).
23. H. Hamster, A. Sullivan, S. Gordon, and R. W. Falcone, "Short-pulse terahertz radiation from high-intensity-laser-produced plasmas," Phys. Rev. E **49**(1), 671–677 (1994).
24. M. Kreß, T. Löffler, M. D. Thomson, R. Dörner, H. Gimpel, K. Zrost, T. Ergler, R. Moshammer, U. Morgner, J. Ullrich, and H. G. Roskos, "Determination of the carrier-envelope phase of few-cycle laser pulses with terahertz-emission spectroscopy," Nat. Phys. **2**(5), 327–331 (2006).
25. M. Kreß, T. Löffler, M. Thomson, H. Roskos, R. Dörner, H. Gimpel, K. Zrost, T. Ergler, R. Moshammer, U. Morgner, and J. Ullrich, "Measurement of the carrier-envelope phase of few-cycle laser pulses by thz-emission spectroscopy," in *Conference on Lasers and Electro-Optics*, (Optical Society of America, 2007), p. CThR4.
26. H. Roskos, M. Thomson, M. Kreß, and T. Löffler, "Broadband THz emission from gas plasmas induced by femtosecond optical pulses: From fundamentals to applications," Laser Photonics Rev. **1**(4), 349–368 (2007).
27. W.-M. Wang, Z.-M. Sheng, H.-C. Wu, M. Chen, C. Li, J. Zhang, and K. Mima, "Strong terahertz pulse generation by chirped laser pulses in tenuous gases," Opt. Express **16**(21), 16999–17006 (2008).
28. H.-C. Wu, J. M. ter Vehn, and Z.-M. Sheng, "Phase-sensitive terahertz emission from gas targets irradiated by few-cycle laser pulses," New J. Phys. **10**(4), 043001 (2008).
29. A. Silaev and N. Vvedenskii, "Residual-current excitation in plasmas produced by few-cycle laser pulses," Phys. Rev. Lett. **102**(11), 115005 (2009).
30. A. P. Shkurinov, A. S. Sinko, P. M. Solyankin, A. V. Borodin, M. N. Esaulkov, V. V. Annenkov, I. A. Kotelnikov, I. V. Timofeev, and X.-C. Zhang, "Impact of the dipole contribution on the terahertz emission of air-based plasma induced by tightly focused femtosecond laser pulses," Phys. Rev. E **95**(4), 043209 (2017).
31. M. Khokhlova and V. Strelkov, "Highly efficient XUV generation via high-order frequency mixing," New J. Phys. **22**(9), 093030 (2020).
32. C. Kan, C. E. Capjack, R. Rankin, and N. H. Burnett, "Spectral and temporal structure in high harmonic emission from ionizing atomic gases," Phys. Rev. A **52**(6), R4336–R4339 (1995).
33. J. Zhou, J. Peatross, M. M. Murnane, H. C. Kapteyn, and I. P. Christov, "Enhanced high-harmonic generation using 25 fs laser pulses," Phys. Rev. Lett. **76**(5), 752–755 (1996).
34. A. Zaïr, M. Holler, A. Guandalini, F. Schapper, J. Biegert, L. Gallmann, U. Keller, A. S. Wyatt, A. Monmayrant, I. A. Walmsley, E. Cormier, T. Auguste, J. P. Caumes, and P. Salières, "Quantum path interferences in high-order harmonic generation," Phys. Rev. Lett. **100**(14), 143902 (2008).
35. E. Brunetti, R. Issac, and D. A. Jaroszynski, "Quantum path contribution to high-order harmonic spectra," Phys. Rev. A **77**(2), 023422 (2008).

Optics EXPRESS

36. W. Cao, G. Laurent, C. Jin, H. Li, Z. Wang, C. D. Lin, I. Ben-Itzhak, and C. L. Cocke, "Spectral splitting and quantum path study of high-harmonic generation from a semi-infinite gas cell," J. Phys. B: At., Mol. Opt. Phys. **45**(7), 074013 (2012).
37. L. He, P. Lan, Q. Zhang, C. Zhai, F. Wang, W. Shi, and P. Lu, "Spectrally resolved spatiotemporal features of quantum paths in high-order-harmonic generation," Phys. Rev. A **92**(4), 043403 (2015).
38. F. Catoire, A. Ferré, O. Hort, A. Dubrouil, L. Quintard, D. Descamps, S. Petit, F. Burgy, E. Mével, Y. Mairesse, and E. Constant, "Complex structure of spatially resolved high-order-harmonic spectra," Phys. Rev. A **94**(6), 063401 (2016).
39. J. Zhang, X.-F. Pan, X. Zhao, J. Guo, K.-G. Zhu, and X.-S. Liu, "Spectral splitting and phase matching of the macroscopic high-order harmonic generation in intense laser fields," J. Opt. **21**(12), 125503 (2019).
40. H. Wang, M. Chini, S. Chen, C. Zhang, F. He, Y. Cheng, Y. Wu, U. Thumm, and Z. Chang, "Attosecond time-resolved autoionization of argon," Phys. Rev. Lett. **105**(14), 143002 (2010).
41. A. D. Shiner, B. E. Schmidt, C. Trallero-Herrero, H. J. Wörner, S. Patchkovskii, P. B. Corkum, J.-C. Kieffer, F. Légaré, and D. M. Villeneuve, "Probing collective multi-electron dynamics in xenon with high-harmonic spectroscopy," Nat. Phys. **7**(6), 464–467 (2011).
42. R. A. Ganeev, C. Hutchison, T. Witting, F. Frank, W. A. Okell, A. Zaïr, S. Weber, P. V. Redkin, D. Y. Lei, T. Roschuk, S. A. Maier, I. López-Quintás, M. Martín, M. Castillejo, J. W. G. Tisch, and J. P. Marangos, "High-order harmonic generation in graphite plasma plumes using ultrashort laser pulses: a systematic analysis of harmonic radiation and plasma conditions," J. Phys. B: At., Mol. Opt. Phys. **45**(16), 165402 (2012).
43. S. Beaulieu, S. Camp, D. Descamps, A. Comby, V. Wanie, S. Petit, F. Légaré, K. Schafer, M. Gaarde, F. Catoire, and Y. Mairesse, "Role of excited states in high-order harmonic generation," Phys. Rev. Lett. **117**(20), 203001 (2016).
44. S. Bengtsson, E. W. Larsen, D. Kroon, S. Camp, M. Miranda, C. L. Arnold, A. L'Huillier, K. J. Schafer, M. B. Gaarde, L. Rippe, and J. Mauritsson, "Space–time control of free induction decay in the extreme ultraviolet," Nat. Photonics **11**(4), 252–258 (2017).
45. M. A. Fareed, V. V. Strelkov, N. Thiré, S. Mondal, B. E. Schmidt, F. Légaré, and T. Ozaki, "High-order harmonic generation from the dressed autoionizing states," Nat. Commun. **8**(1), 16061 (2017).
46. S. Beaulieu, E. Bloch, L. Barreau, A. Comby, D. Descamps, R. Géneaux, F. Légaré, S. Petit, and Y. Mairesse, "Phase-resolved two-dimensional spectroscopy of electronic wave packets by laser-induced XUV free induction decay," Phys. Rev. A **95**(4), 041401 (2017).
47. C. Serrat, "Coherent extreme ultraviolet light amplification by strong-field-enhanced forward scattering," Phys. Rev. Lett. **111**(13), 133902 (2013).
48. C. Reinhardt, B. Chichkov, and B. Wellegehausen, "Self-induced parametric amplification of high-order harmonics," Opt. Lett. **25**(14), 1043–1045 (2000).
49. L. V. Dao, K. B. Dinh, and P. Hannaford, "Perturbative optical parametric amplification in the extreme ultraviolet," Nat. Commun. **6**(1), 7175 (2015).
50. J. Seres, E. Seres, D. Hochhaus, B. Ecker, D. Zimmer, V. Bagnoud, T. Kuehl, and C. Spielmann, "Laser-driven amplification of soft x-rays by parametric stimulated emission in neutral gases," Nat. Phys. **6**(6), 455–461 (2010).

134.214.242.85 {ts '2021-02-11 04:23:03'}